Human Molecular Genetics, 2019, Vol. 28, No. 6 961–971

doi: 10.1093/hmg/ddy397
Advance Access Publication Date: 22 November 2018
General Article

GENERAL ARTICLE

Human SPG11 cerebral organoids reveal cortical neurogenesis impairment

Francesc Pérez-Brangulí[1,‡,*], Isabel Y. Buchsbaum[2,3,‡], Tatyana Pozner[1,‡], Martin Regensburger[1,4], Wenqiang Fan[6], Annika Schray[1], Tom Börstler[1], Himanshu Mishra[1], Daniela Gräf[1], Zacharias Kohl[5,8], Jürgen Winkler[5,8], Benedikt Berninger[6,7], Silvia Cappello[2,*] and Beate Winner[1,8,*,†]

[1]Department of Stem Cell Biology (former IZKF junior research group III), Friedrich–Alexander-Universität Erlangen–Nürnberg (FAU), Erlangen, Germany, [2]Max-Planck Institute of Psychiatry, Munich, Germany, [3]Graduate School of Systemic Neurosciences (GSN), Ludwig-Maximilians University (LMU), Planegg/Martinsried, Germany, [4]Department of Neurology, Friedrich–Alexander-Universität Erlangen–Nürnberg (FAU), Erlangen, Germany, [5]Department of Molecular Neurology, Friedrich–Alexander-Universität Erlangen–Nürnberg (FAU), Erlangen, Germany, [6]Adult Neurogenesis and Cellular Reprogramming, Institute of Physiological Chemistry and Focus Program Translational Neuroscience, University Medical Center, Johannes Gutenberg University Mainz, Mainz, Germany, [7]Institute of Psychiatry, Psychology & Neuroscience, Centre for Developmental Neurobiology and MRC Centre for Neurodevelopmental Disorders, King's College London, London, UK and [8]Zentrum für Seltene Erkrankungen Erlangen (ZSEER), Friedrich–Alexander-Universität Erlangen–Nürnberg (FAU), Erlangen, Germany

*To whom correspondence should be addressed. Beate Winner, Tel: +49-9131-85-39301; Fax: +49-9131-85-39311; Email: beate.winner@fau.de; Francesc Pérez-Brangulí, Email: fpbranguli@gmail.com and Silvia Cappello, Tel: +49-89-30622253; Fax: +49-89-30646639; Email: silvia_cappello@psych.mpg.de

Abstract

Spastic paraplegia gene 11(SPG11)-linked hereditary spastic paraplegia is a complex monogenic neurodegenerative disease that in addition to spastic paraplegia is characterized by childhood onset cognitive impairment, thin corpus callosum and enlarged ventricles. We have previously shown impaired proliferation of SPG11 neural progenitor cells (NPCs). For the delineation of potential defect in SPG11 brain development we employ 2D culture systems and 3D human brain organoids derived from SPG11 patients' iPSC and controls. We reveal that an increased rate of asymmetric divisions of NPCs leads to proliferation defect, causing premature neurogenesis. Correspondingly, SPG11 organoids appeared smaller than controls and had larger ventricles as well as thinner germinal wall. Premature neurogenesis and organoid size were rescued by GSK3 inhibititors including the Food and Drug Administration-approved tideglusib. These findings shed light on the neurodevelopmental mechanisms underlying disease pathology.

[†]Beate Winner, http://orcid.org/0000-0002-6909-0564
[‡]These authors contributed equally to this work.
Received: July 6, 2018. **Revised:** October 23, 2018. **Accepted:** November 10, 2018

Introduction

Mutations in *ALS5/SPG11/KIAA1840*-encoding SPATACSIN cause a spectrum of neurodevelopmental and neurodegenerative diseases including the most frequent form of autosomal recessive hereditary spastic paraplegia (HSP) (36), termed spastic paraplegia gene 11 (SPG11), young onset amyotrophic lateral sclerosis (ALS5) (28) and Charcot–Marie–Tooth disease (CMT1a) (26). Spatacsinopathies converge a clinical spectrum ranging from cognitive impairment and thin corpus callosum (TCC) to spastic paraplegia and peripheral motor neuropathy. This multisystemic involvement points towards distinct temporal and spatial, yet incompletely understood functions of SPATACSIN. The prominent nervous system involvement in *SPG11*-linked HSP is connected to SPATACSIN's active temporal and spatial expression throughout the nervous system. The neurodegenerative phenotype was linked to autophagy: together with another HSP-related protein (ZFYVE26), the *SPG11* protein SPATACSIN is instrumental for the reformation of lysosomes from autophagolysosomes, i.e. a recycling pathway that generates new lysosomes (7,39).

Among others, SPG11-HSP belongs to a subset of complex forms of HSPs characterized by TCC and is often associated with cognitive impairment (15), indicative of a neurodevelopmental defect. In conjunction, a majority of SPG11 patients show mild to severe enlargement of the lateral ventricles and of the cerebral sulci, in addition to a TCC and diffuse white matter hyperintensity (31).

The functional role of *SPG11* in neurodevelopmental alterations remains largely unexplored. Induced pluripotent stem cell (iPSC)-derived neuronal models have been decisive for characterizing the cellular phenotypes of neurodevelopmental deficits in autism, Rett syndrome and Williams syndrome (6,22,23). We have previously described a proliferation deficit in neural progenitor cells (NPCs) derived from SPG11 patients' iPSC (25). More recently, 3D iPSC-derived organoid systems opened the opportunity to model brain diseases in a system with remarkable similarities to human organogenesis (18,24,34).

Here, we took advantage of the cerebral organoid system and of live-cell imaging to recapitulate the temporal and spatial pattern of NPC division and differentiation in SPG11-HSP patients. Using 2D and 3D culture conditions, namely differentiating NPCs, neurospheres and cerebral organoids, we identified an increased asymmetric division in SPG11-NPCs at the germinal zone of cortical ventricles at the expense of symmetric division. This impairment in self-renewal contributes to the premature generation of cortical neuroblasts and neurons and is dependent on GSK3 signaling. Inhibition of GSK3 activity using the Food and Drug Administration (FDA)-approved compound tideglusib is sufficient to rescue premature neurogenesis and more importantly increases organoid size in SPG11. Our data provide insights into how *SPG11* alters neurodevelopment and further links this disease to the group of neurodevelopmental disorders. Moreover, we provide a proof of concept that 3D brain organoids are valuable tools for precision medicine.

Results

SPG11 patients and controls included in the study

The SPG11-HSP patients reported in this study are characterized by an early onset of cognitive impairment in the first and second decade (15). In total, we derived iPSC from three patients (two lines each), referred to as SPG11-1, SPG11-2 and SPG11-3. SPG11-1 and SPG11-2 are sisters with compound heterozygous mutations c.3036C>A/ p.Tyr1012X in exon 16 and c.5798 delC/ p.Ala1933ValfsX18 in exon 30. SPG11-3 has compound heterozygous mutations at c.267G>A/ p.Trp89X in exon 2 and at 1457-2A>G in intron 6 (splice site mutation corresponding to the previously reported mutation c.1757-2A>G) (15). The detailed clinical, genetic and imaging characteristics of the patients were previously published (15). The controls are two age-matched healthy Caucasian individuals with no history of movement disorder or neurologic disease.

SPG11-NPCs display an altered self-renewal pattern in cerebral organoids

To experimentally mimic the temporal and spatial division of neural cells in SPG11 patients and controls, we generated and analyzed cerebral organoids derived from iPSC. The size of organoids derived from SPG11-iPSC (SPG11 organoids) was significantly smaller compared to controls during early development of the organoids (6 days) and was not compensated over time (6 weeks, Fig. 1A and B). Organoids developed a structural organization into germinal zones and cortical regions (Fig. 1C; Supplementary Material, Fig. S1A). Germinal zones of SPG11 organoids cultured for both 6 and 9 weeks contained significantly less proliferating phospho-histone H3 positive ($PH3^+$) cells when compared to controls (Fig. 1D, E and G). The thickness of the progenitor zone was significantly reduced in SPG11 organoids after 9 weeks, but not at 6 weeks (Fig. 1F and H), indicating that fewer dividing cells impact the thickness of the germinal wall already at 6 weeks (young organoid stage). In addition, the lumen of the ventricles appeared larger in SPG11 organoids compared to controls (Fig. 1D). It is important to note that cell death levels did not differ between controls and SPG11 organoids (Supplementary Material, Fig. S5), possibly due to a constant rate of ongoing cell death occurring in cerebral organoids model (21).

While vertically dividing NPCs in the apical ventricular zone result in two daughter cells (symmetric division), horizontal (asymmetric) divisions give rise to one stem cell and one neuroblast (13,27). Spindle orientations were evaluated by analyzing division angles of nuclear mitotic apparatus-positive cells in the progenitor zone of organoids. We found a significantly increased amount of horizontally dividing cells at the expense of vertically dividing cells in SPG11 organoids, indicating a shift towards asymmetric division in SPG11 (Fig. 1I and J). We also noticed structural changes in the ventricular zone; while the apico-basal polarity was correctly established as shown by ß-catenin (ßCat) staining next to the ventricle-like lumen, the progenitor zone and the cortical plate were less clearly separated as visible by more neuroblasts within the progenitor zone in SPG11 organoids (Fig. 1D; Supplementary Material, Fig. S1B and C).

Longer cell cycle duration in SPG11-NPCs

To explore the duration and the frequency of cell division, we carried out single-cell tracking time-lapse microscopy in SPG11- and control-NPCs (Supplementary Material, Fig. S1D). SPG11-NPCs underwent lesser divisions than controls after 6 days in culture (Supplementary Material, Fig. S1E). To follow the fate of individual cells and their progeny, single-cell tracking of GFP-labeled NPCs was performed acquiring phase contrast

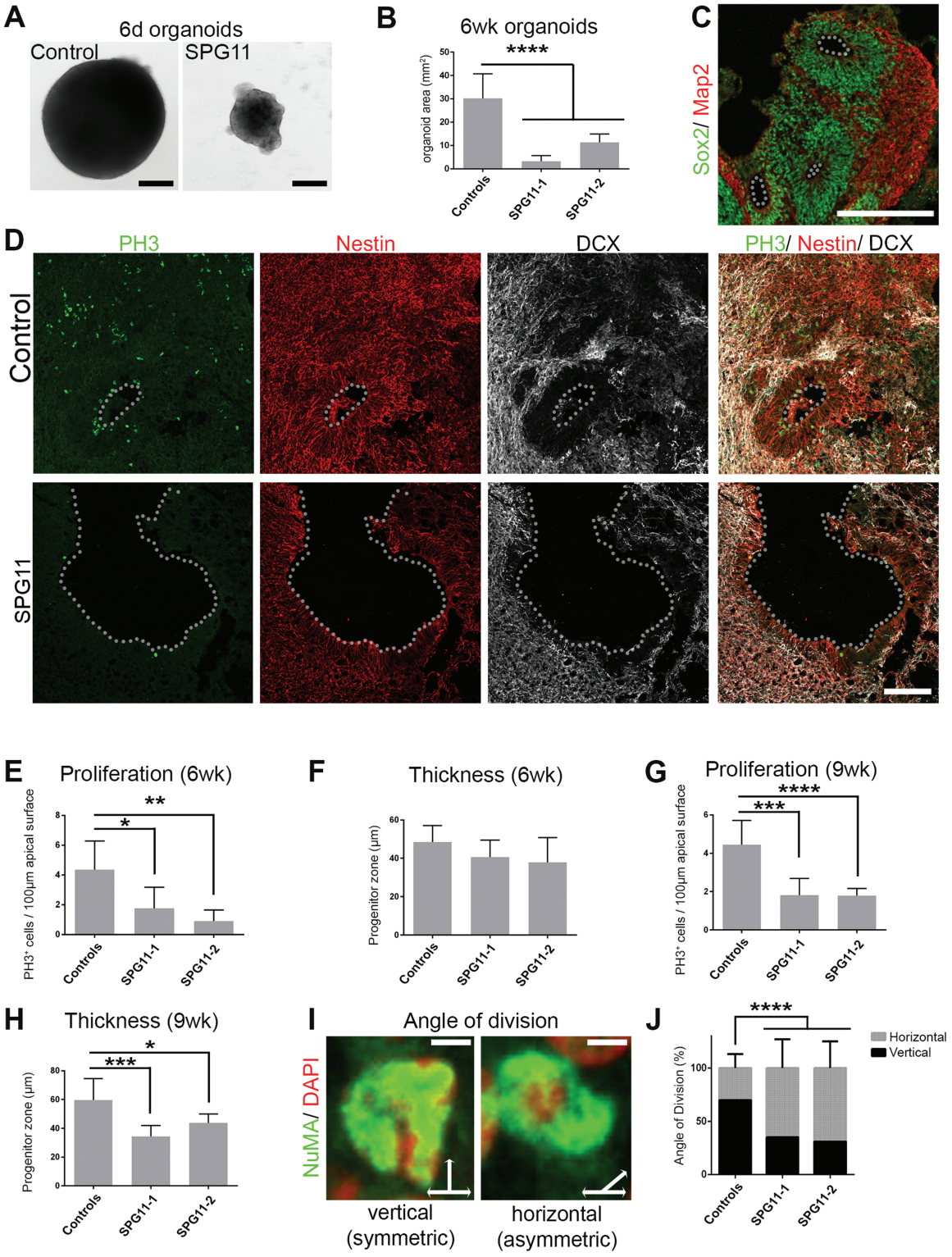

Figure 1. Altered size and self-renewal pattern in SPG11 organoids. **(A)** Representative bright field images of 6-day-old cerebral organoids generated from SPG11- and control-iPSCs. **(B)** Significant decrease in total organoid size in SPG11 at 6 weeks (****$P < 0.0001$; $n \geq 9$ organoids per group). **(C)** Control cerebral organoids with apical progenitor zones ($Sox2^+$, green) and basal neurons ($Map2^+$, red). **(D)** Cerebral organoids from control- and SPG11-iPSCs, cultured for 9 weeks. PH3 (green): proliferating cells, nestin (red): NPCs, DCX (grey): neuroblasts. Apical surface indicated by dotted lines. Quantification of **(E–H)** $PH3^+$-cells in the progenitor zone per 100 µm apical surface length, progenitor zone thickness (µm) of 6-week-old **(E, F)** and 9-week-old **(F, H)** organoids, respectively (*$P < 0.05$, **$P < 0.01$, ***$P < 0.001$, ****$P < 0.0001$; $n \geq 5$ organoids per group). **(I)** Orientation of $NuMA^+$ cells (green): horizontal and vertical divisions (micrographs exemplify angle of division). Nuclei labeled with DAPI (red). **(J)** Percentage of $NuMA^+$ cells undergoing horizontal and vertical division at the ventricle wall of 6-week-old organoids (****$P < 0.0001$; $n \geq 200$ cells per group). Controls were grouped in (B), E–J). All data: mean ± SD. Scale bars: 200 µm in (A), (C), (D). 5 µm in (I).

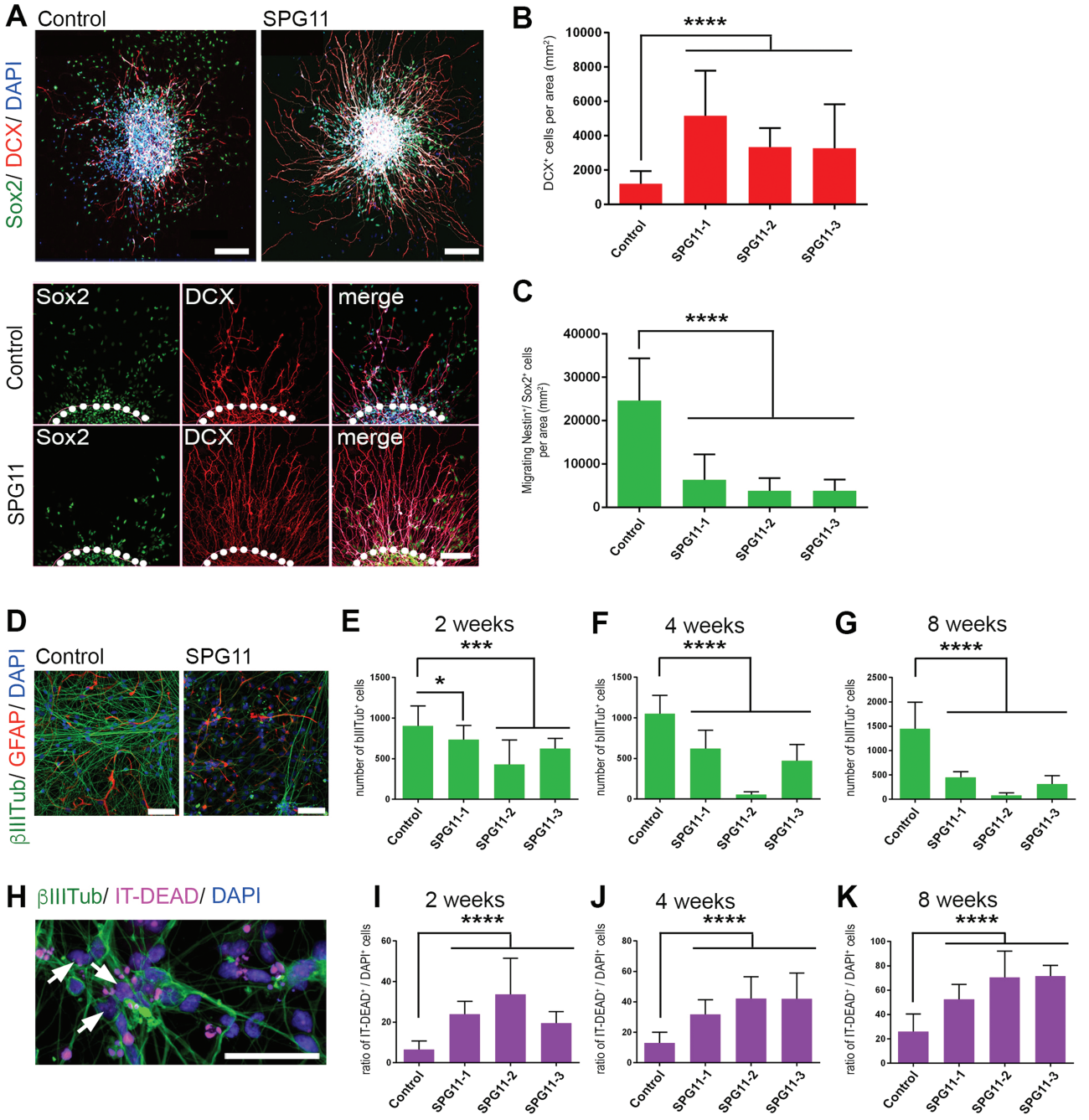

Figure 2. SPG11-NPCs undergo premature neurogenesis. **(A)** NPC spheres from controls and SPG11 patients; NPCs (green) and neuroblasts (red) were labeled with anti-Sox2 and anti-DCX, respectively. **(B, C)** Quantification of migrating DCX^+- and $Sox2^+$-cells in relation to the area of the assessed spheres (dotted lines: borders of the analyzed area; **** $P < 0.0001$ for all comparisons of control versus SPG11-1, SPG11-2, and SPG11-3; $n \geq 24$ spheres per group). **(D)** Neuronal differentiation of NPCs, labeled for the neuronal marker ßIIITubulin (ßIIITub; green), the astrocyte marker GFAP (red), and DAPI (blue). **(E–G)** The numbers of ßIIITub$^+$-cells are significantly decreased in SPG11 patients' lines at 2, 4 and 8 weeks of differentiation when compared to control (* $P < 0.05$, *** $P < 0.001$, **** $P < 0.0001$; $n \geq 10$ per group). **(H)** Neuronal differentiation of NPCs, labeled for ßIIITub (green) and the cell death dye IT-DEAD (magenta), DAPI (blue). Arrows indicate dead neurons. **(I–K)** Significantly increased numbers of dead cells in SPG11 cortical cultures at 2 (I), 4 (J) and 8 (K) weeks in culture (**** $P < 0.0001$ for all comparisons of control versus SPG11-1, SPG11-2, and SPG11-3; $n \geq 26$ per group). All data: mean ± SD. Scale bars: 200 µm [overview (A)] and 50 µm [magnification (A), (D) and (H)].

and fluorescent images every 8 and 160 min, respectively. The temporal analysis showed significantly reduced division rounds per clone in SPG11-NPCs (Supplementary Material, Fig. S1F and G) and delineated that SPG11-NPCs need more time to complete a full-cell cycle (Supplementary Material, Fig. S1H).

Premature neurogenesis in SPG11-NPCs

To evaluate changes in migration and neuronal differentiation in NPCs, we analyzed neural stem cell (Sox2/Nestin) and neuroblast markers (DCX) in NPCs growing in spherical structures under mitogenic culture conditions as neurospheres (3). When

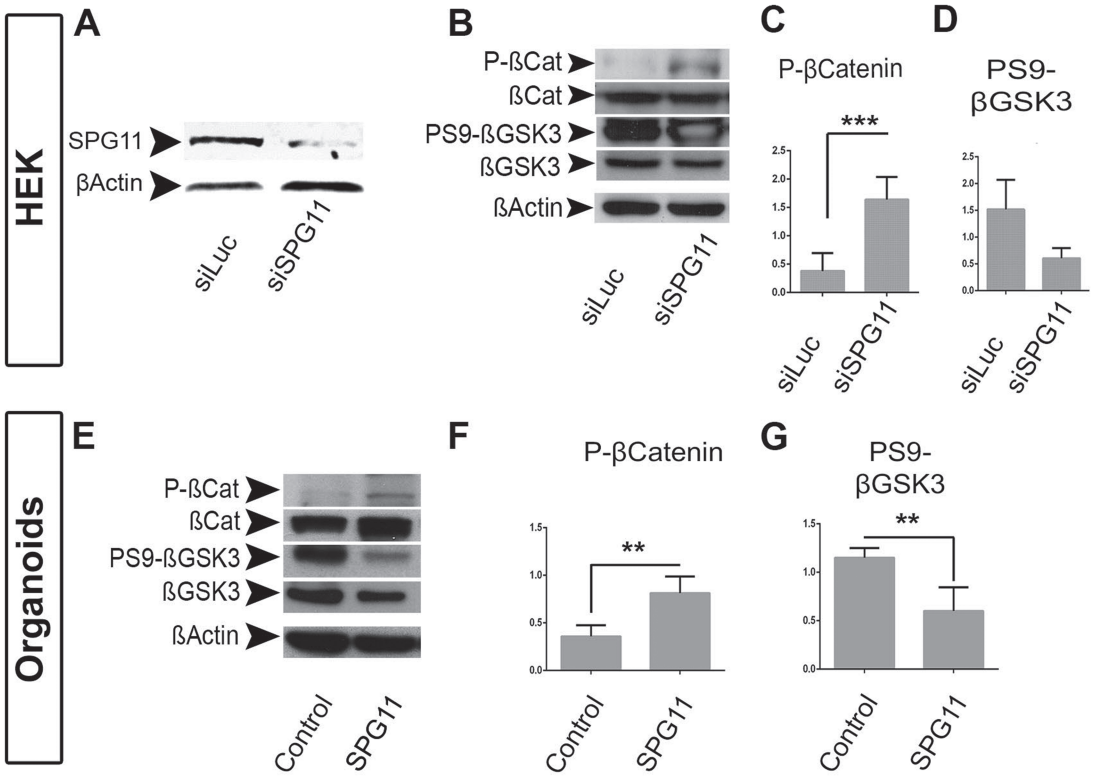

Figure 3. GSK3 overactivation in SPG11. **(A–E)** HEK cells transfected with control siRNA (siLuc) and siRNA against spatacsin (siSPG11). β-Actin served as loading control. **(A)** Demonstration of spatacsin knockdown in HEK cells upon siSPG11 transfection, but not siLuc transfection. **(B)** Western blots of hyperphosphorylated βCat (P-βCat), total βCat, inactivated (PS9-βGSK3) and total βGSK3. **(C)** Quantification of P-βCat. Data were related to total βCat (***$P < 0.001$; $n = 3$). **(D)** Quantification of PS9-βGSK3, related to total βGSK3 (no significant change; $n = 3$). **(E)** Western blots of protein preparations of untreated control- and SPG11-organoids, blotted for the same proteins as in (B). **(F)** Quantification of P-βCat in control- and SPG11-organoids. Data were related to total βCat (**$P < 0.01$; $n = 3$). **(G)** PS9-βGSK3 in control- and SPG11-organoids. Data were related to total βGSK3 (**$P < 0.01$; $n = 3$). All data: mean ± SD.

quantifying cells migrating out from the sphere borders 48 h after plating, significantly more DCX^+-cells were present in the SPG11 groups, indicating an increased number of migrating neuroblasts (Fig. 2A and B). As expected, the number of Sox2-positive NPCs was significantly reduced in SPG11, while no GFAP-positive cells were present (Fig. 2A and C; Supplementary Material, Fig. S2A). This indicates an increase of migrating neuroblasts at the expense of NPCs, which is in line with the shift in division towards an asymmetric pattern in organoids.

To test if premature neurogenesis, associated with the dysfunction of *SPG11*, implies a decrease in the total number of neurons, we induced neuronal differentiation in SPG11-NPCs. Compared to controls, SPG11-NPCs differentiated for 2, 4 and 8 weeks showed a severe reduction of neurons (Fig. 2D–G) and significantly increased rates of cell death (Fig. 2H–K). The number of GFAP-positive astrocytes was unchanged in weeks 2 and 4. There was a significant increase in GFAP-positive astrocytes at week 8 (Supplementary Material, Fig. S2B).

Partners for the modulation of neurogenesis in spatacsinopathies

SiRNA-mediated knockdown of *SPG11* was performed to model SPATACSIN loss of function in HEK cells (Fig. 3A). P-ßCat levels were significantly increased upon SPG11-siRNA transfection when compared to control luciferase-siRNA transfection (Fig. 3B and C). βGSK3 activity is regulated by phosphorylation at specific sites and phosphorylation of serine-9 (PS9-βGSK3) results in inactivation (16). In *SPG11*-silenced cells, despite a trend, the inactivated form of βGSK3 (PS9-βGSK3) was unaltered (Fig. 3D).

Since this result might have been influenced by the cell type (HEK cells) used for the analysis and to proceed towards the crucial step of translating these findings into precision medicine, knowledge about the biochemical changes in complex neural models is essential. We thus analyzed components of the GSK3/βCat pathway in SPG11 organoids. Dysregulation of βGSK3 was also observed in SPG11 organoids, i.e. P-ßCat levels were increased and PS9-βGSK3 levels were significantly decreased (Fig. 3E–G).

Phosphorylated cAMP response element-binding protein (pCREB) is a key factor in the regulation of neurogenesis (12) and previous studies described a direct interaction between pCREB and three amino acids in βGSK3 (17). We therefore investigated, if activated CREB (Supplementary Material, Fig. S3A and B) is altered in SPG11-NPCs. We found a significant increase in SPG11-NPCs, indicative of increased transcription of neurogenic genes (20). These findings imply that premature activation of neurogenesis in SPG11 was driven by a concomitant repression of proliferative pathways of the Wnt/ßCat system.

Modulation of the GSK3/β-catenin pathway rescues SPG11 phenotypes

In a first step, we investigated how the premature neurogenesis phenotype in SPG11 can be rescued. We first tested in SPG11- and

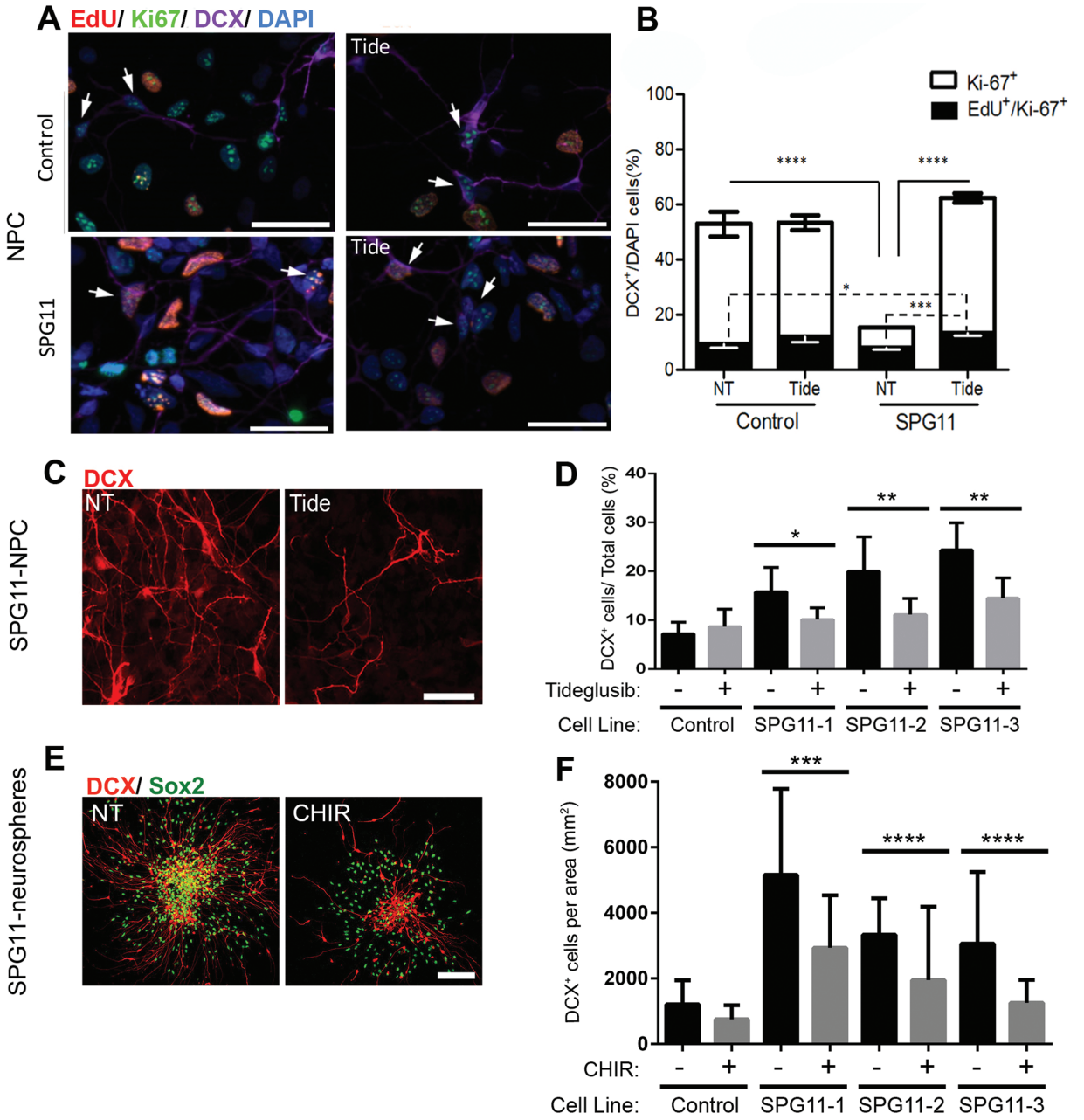

Figure 4. Rescue of premature neurogenesis in SPG11-NPCs. **(A)** Images of untreated (left) and tide-treated (right) control- and SPG11-NPCs. The cells were stained for EdU (orange), Ki-67 (green) and DCX (purple). Proliferating cells are indicated with arrows. **(B)** Quantification of the percentage of Ki-67-positive cells out of DCX-positive cells, with representation of the subpopulation of EdU/Ki-67/DCX-positive cells within the proliferative population of neuroblasts (DCX^+). **(C)** Images of SPG11-NPCs, untreated (NT) or treated with tideglusib (Tide) and stained for DCX (red). **(D)** Quantification of the percentage of neuroblasts (DCX^+) in relation to the total number of cells. Three control NPC lines (grouped) and SPG11-NPC lines (SPG11-1 and SPG11-2, SPG11-3, respectively) were analyzed ($n \geq 20$ per condition). **(E)** Non-treated (NT) and CHIR-treated neurospheres generated from SPG11-NPCs, labeled with DCX (red) and Sox2 (green). **(F)** Quantification of DCX^+-cells in NT or CHIR-treated spheres per mm^2 ($n \geq 20$ per condition). $^*P < 0.05$; $^{**}P < 0.01$; $^{***}P < 0.001$; $^{****}P < 0.0001$. Data in (D), (F): mean ± SD; data in (B): mean ± SEM. Scale bars: 50 µm.

control-NPCs whether overexpression of SPATACSIN was able to rescue premature neurogenesis. Overexpression of SPATACSIN reduced the number of DCX^+-cells in SPG11-NPCs under proliferating conditions (Supplementary Material, Fig. S3C–E), indicating that restoration of SPATACSIN levels can revert the phenotype. To further examine proliferation of SPG11 neuroblasts, we labeled NPCs with EdU 1 h before harvesting (paradigm: Supplementary Material, Fig. S4B). We then counted EdU/KI67/DCX-positive cells within the total population of KI67/DCX double positive cells. While the percentage of total Ki-67/DCX double positive cells was decreased in SPG11 neurons, there was no significant difference in the EdU-positive subpopulation of the proliferating neuroblasts (EdU/Ki-67/DCX-positive cells; Fig. 4A and B).

We next asked whether the observed phenotype can be rescued by manipulation of the βGSK3 pathway. For this aim

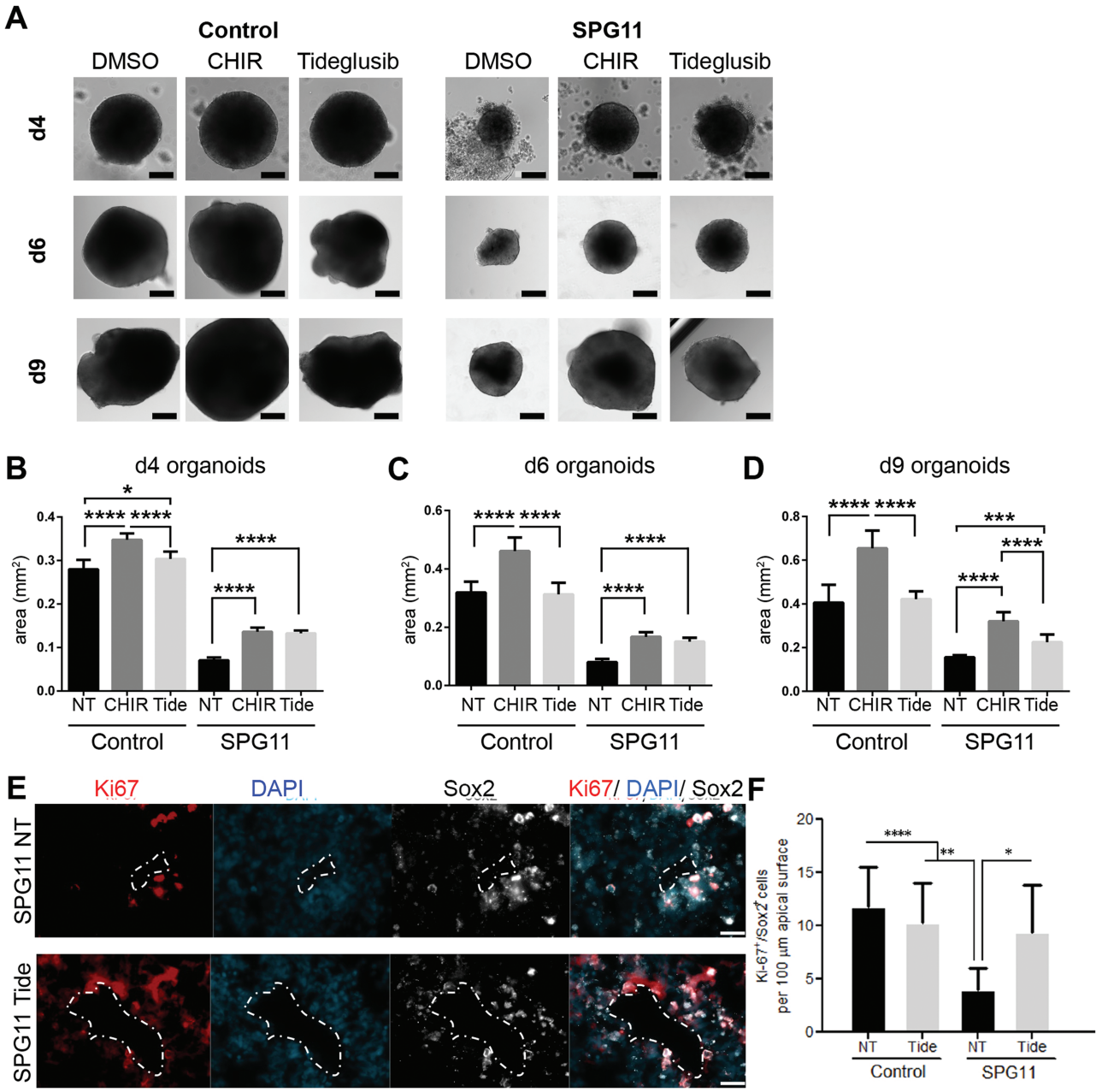

Figure 5. Rescue of SPG11 phenotypes in organoids. **(A)** Bright field images of control- and SPG11-organoids, NT or treated with CHIR or Tide, at 4, 6 and 9 days in culture. **(B–D)** Quantification of organoid size at day 4, 6 and 9 for the respective groups. **(E)** Organoids (40d) stained for Ki-67 (red) and Sox2 (white). **(F)** Quantification of 40d organoid proliferation (treated according to the paradigm in Supplementary Material, Fig. S4D; $^{*}P < 0.05$, $^{**}P < 0.01$ $^{***}P < 0.001$, $^{****}P < 0.0001$; (A–C): $n \geq 9$ organoids per condition; E-F: $n \geq 3$). All data: mean ± SD. Scale bars: 200 µm in (A); 20 µm in (E).

we employed compounds that specifically inhibit βGSK3, an FDA-approved tideglusib and CHIR. We found that tideglusib was able to increase the number of proliferating neuroblasts in SPG11. (Fig. 4A and B). Interestingly, tideglusib or CHIR treatment reduced the premature generation of neuroblasts in SPG11-NPCs (Fig. 4C and D) and in neurosphere model, respectively (Fig. 4E and F; paradigms Supplementary Material, Fig. S4).

In summary, in addition to the rescue of SPATACSIN loss of function by overexpression, also pharmacological inhibition of ßGSK3 decreased neuroblast numbers and thus attenuated premature neurogenesis in SPG11-NPCs.

When treating organoids with CHIR or tideglusib (paradigm Supplementary Material, Fig. S4D), SPG11 organoids significantly increased in size compared to untreated controls (Fig. 5A–D). We conclude that decreased organoid size in SPG11 is partially rescued by ßGSK3 inhibition. CHIR had effects on both control- and SPG11-organoid sizes. Interestingly, tideglusib specifically increased the size of SPG11 organoids, but did not influence organoid size of controls. Moreover, the significantly lower amount of Ki-67^{+}/Sox2^{+} cells at the apical surface of SPG11 organoids compared to controls was rescued by tideglusib treatment (Fig. 5E and F). This indicates that tideglusib might be a potent compound for SPG11 in 3D structures.

Discussion

We employed iPSC-derived multidimensional neuronal cultures of SPG11 patients to demonstrate that disruption of SPATACSIN leads to impaired self-renewal of cortical NPCs, resulting in premature neurogenesis due to an increase in asymmetric versus symmetric division and consequently a progressively reduced survival of neurons. The addition of an FDA-approved βGSK3 modulator (tideglusib) increased organoid size in SPG11.

Although animal models have provided insights into SPG11, specifically early onset pathologies are inconsistent; a previously published *SPG11*-null mouse, generated by inserting a gene-trap cassette in the first exon of the *SPG11* gene, exclusively showed late-onset motor impairments, together with a massive loss of neurons in the cortex and cerebellum of old mice (39). In contrast, the disruption of *SPG11* by introduction of a stop codon in exon 32, mimicking the most frequent mutation observed in SPG11 patients, resulted in early cognitive deficits, together with abnormal callosal projections and neuronal death in the cortex of mutant mice (2). This considerable variability reflects the need for alternative strategies to decipher the function of spatacsin in human models.

The invention of generating iPSCs opened the unique possibility of modeling disease phenotypes in a human cellular system (38). IPSC-derived 3D neuronal models, so-called cerebral organoids, mimic fetal development and hold great promise of providing the spatial and temporal solution for elucidating disease mechanisms (5,18). Our findings parallel cellular neurodevelopmental phenotypes recently described in human cerebral organoids of severe lissencephalies such as the Miller–Dieker syndrome (1) or other microcephalies (18). Changes at the NPC stage may represent the cellular phenotype of cortical atrophy observed in SPG11 patients. Traditionally considered as a neurodegenerative disease with juvenile onset, cortical MRIs of SPG11 patients evidenced early reductions of grey matter volumes (37). These imaging studies were complemented by the *post-mortem* finding of severe neuronal loss in the frontal cortex of SPG11 patients (10). Specifically, TCC and childhood onset atrophy of the cortex, combined with early-onset cognitive impairment might be characteristic of early childhood onset in SPG11 patients. Our finding that dysfunction of *SPG11* interferes with the development of iPSC-derived brain organoids is in line with early cortical atrophy diagnosed in the patients included in this study (15). Our data thus support the hypothesis of an additional neurodevelopmental phenotype in SPG11-HSP.

Our results in SPG11 iPSC-derived neural models suggest a reduced rate of symmetric division of NPCs, a higher proportion of proliferative neuroblasts and defects in the germinal zone of organoids, which ultimately result in premature neurogenesis (Fig. 5G). More specifically, we observe defects at two distinct stages. First of all, SPG11-NPCs present with longer cell cycle, which is complemented by increased asymmetric division rate, resulting in increased number of neuroblasts, or premature neurogenesis. For instance, rodent models revealed interplay between the duration of the cell cycle and the initiation and the total period of neurogenesis (4). A prolonged duration of mitosis was previously connected to premature neuronal differentiation of radial glia cells and an increase in apoptotic cells in a murine model of mago homolog, exon junction complex core component *Magoh* (33). Likewise, in humans, disease-causing mutations have helped to identify molecular mechanisms of cell cycle and neurogenesis regulation. For example, the *protocadherin 19* gene, mutated in intellectual disability, modulates neurogenesis via excessively prolonged mitosis of progenitors (9). Second, at neuroblast stage, there are less proliferating cells, possibly due to premature differentiation. Overall, the combination of these defects culminated in defective SPG11 neurons (Supplementary Material, Fig. S6).

SPATACSIN was previously linked to a significant decrease of axon-related genes and neurite complexity (32). Activated GSK3 is implicated in neurogenesis, promoting the degradation of ßCat and the activation of an array of transcription factors like CREB, but also in glutamate-induced neuronal death (8). Therefore, our results point out that the dysfunction of SPATACSIN impairs the delicate balance of the GSK3 signaling system. The activation of GSK3, in turn, significantly contributes to changes in NPC proliferation, neurogenesis and neuronal maturation (11). Our previous observations in SPG11-NPCs indicated impaired ßCat signaling in SPG11-NPC that could be rescued by administration of specific βGSK3 inhibitors (25). We took advantage of this knowledge in order to assess whether the same observations are present also in the neurosphere and cerebral organoids models. Along this line, two different GSK3 inhibitors (CHIR and tideglusib) reversed neurodevelopmental defects in SPG11 cortical cultures, and organoids. Tideglusib, an FDA-approved drug, improved cognitive function in mild Alzheimer's Disease (19) and is currently in phase II clinical studies for adolescents with autism spectrum disorder and myotonic dystrophy (clinicaltrials.gov). Tideglusib therefore appeals as a promising compound based on its specificity in blocking ßGSK3, which is the isoform distinctively implicated in proliferation/neurogenesis tasks, and thereby rescuing SPG11 neurodevelopmental phenotypes. Furthermore, since the blockade of GSK3 also activates lysosomal/autophagy pathways (30), tideglusib might also attenuate aberrant accumulation of membranous bodies associated with dysfunction of *SPG11* (35).

Our previous study indicated the beneficial effect of βGSK3 inhibition on NPCs. Here, for the first time we link SPG11/SPATACSIN in their roles for the Wnt/ßCat pathway in a 3D brain organoid system. By confirming the potency of tideglusib in a complex, human brain organoid system we emphasize the clinical relevance of the compound.

In addition, our findings are the first report to decipher impaired cortical neurogenesis in SPG11-HSP. We provide a rigorous spatial and temporal analysis of the related pathology in 2D and 3D systems. Alterations of the natural ratio of cell divisions and proliferation rate are tightly linked to the observed morphological changes of brain organoids. These observations are crucial for the understanding of disease etiology and contribute a novel aspect for clinical intervention.

Experimental procedures

SPG11 patients and controls

Three patients (UKERi6O6-R1, UKERi4AA-R1 and UKERiK22-R1, described as SPG11-1, SPG11-2 and SPG11-3) and two controls (UKERi1JF-R1 and UKERi1E4-R1) were included. Patients were described in detail previously (15). The underlying Institutional Review Board approval (Nr. 4120: *Generierung von humanen neuronalen Modellen bei neurodegenerativen Erkrankungen*) and informed consent were obtained at the movement disorder clinic at the Department of Molecular Neurology, Universitätsklinikum Erlangen (Erlangen, Germany).

IPSC-derived neuronal model

IPSCs were reprogrammed from fibroblasts using Yamanaka's retroviral transduction (two iPSC lines per individual). The lines were maintained and controlled for pluripotency as previously described (14). From every individual, two independent NPC lines and respective neurons were generated using an embryoid body (EB)/rosette protocol (14) and further differentiated into neurons.

Multidimensional cultures

Cerebral organoids were generated from iPSC as previously described (18). For control lines, EBs were generated from 9000 cells each. For patient lines, EBs were generated from 9000 and 18 000 cells with no visible difference in size or development. Two control- and two SPG11-iPSC lines (SPG11-1 and SPG11-2) were analyzed. Controls were grouped. Cerebral organoids were cultured for 40 to 61 days (6 and 9 weeks) at 37°C under 5% CO_2 and atmospheric oxygen. For the rescue experiment, control- and SPG11 organoids were treated with 1 µM of the GSK3 blockers CHIR99021 and tideglusib and kept in culture for 40 to 60 days (6 and 9 weeks). Compounds were replaced every 2–3 days (Supplementary Material, Fig. S4D).

For the neurosphere assay (3), NPCs were kept in suspension in 96 well ultra-low attachment plates (Corning, Amsterdam, the Netherlands) for 72 h at a density of 5×10^4 cells/cm^2 under proliferative conditions. For the analysis of NPC migration, neurospheres grew attached to polyornithine/laminin (Invitrogen, Carlsbad, California, United States) coated coverslips for 48 h (Fig. 2A). Spheres generated from six SPG11-NPC lines (SPG11-1, SPG11-2 and SPG11-3) were compared to controls.

Time-lapse video microscopy

Control- and SPG11-NPCs were infected with a pEF1-GFP lentivirus. Time-lapse assays were performed for 6 days under mitogenic conditions. Time-lapses and single-cell tracking (29) of SPG11- and control-NPCs were performed with a cell observer (Zeiss Jena, Germany) at 37°C and 5% CO_2. Phase contrast and fluorescent images were acquired every 8 and 160 min respectively using a 20× phase contrast microscopy objective (Zeiss), an AxioCam HRm camera and Zeiss AxioVision 4.7 software (Zeiss). Time-lapses were assembled using ImageJ whereas single-cell tracking was carried out using a self-written computer program (TTT). Per every assessed NPC line, at least 40–50 videos were analyzed and 50 single cells tracked. Time-lapse analyses were evaluated from two control- and three SPG11-NPC lines (SPG11-1, SPG11-2 and SPG11-3). Control NPC lines were grouped.

Statistical analysis

Immunofluorescence analyses, neurite measurement, protein expression and phosphorylation were statistically analyzed using Prism (GraphPad, San Diego, California, United States). Unless indicated otherwise, all data are shown as mean ± SD. Statistical analysis was carried out employing the Student's *t*-test for unpaired variables (two-tailed) and one-way *analysis of variance* followed by Bonferroni multiple comparison tests when three or more groups were compared. *P*-values < 0.05 were considered significant.

Detailed information on the transfection of human cells and details for immunofluorescence, protein sample preparation and western blot assays are listed in the supplemental methods.

Supplementary Material

Supplementary Material is available at *HMG* online.

Acknowledgements

This work is dedicated to our patients, whom we have been following up for more than 15 years now, controls and is *in memoriam* of Anne Wahlig. We thank Professor Chichung Lie, Timucin Öztürk, Dr Iryna Prots, Holger Wend and Dr Marisa Karow for excellent support and critical input.

Conflict of Interest statement. None declared.

Funding

Tom-Wahlig Foundation Advanced Fellowship; German Federal Ministry of Education and Research (BMBF: 01GQ113, 01GM1520A, 01EK1609B); Deutsche Forschungsgemeinschaft (GRK2162 to M.R., T.P., J.W., B.W., CA 1205/2-1 to S.C.); Interdisciplinary Centre for Clinical Research (University Hospital Erlangen; N3 to B.W., J52 to M.R.); Bavarian Ministry of Education and Culture, Science and the Arts in the framework of the Bavarian Research Network for Molecular Biosystems (BioSysNet); Bavarian Network for induced pluripotent stem cells (ForIPS).

Author contributions

F.P.B., I.Y.B., S.C. and B.W. participated in the conceptualization. F.P.B., I.Y.B, T.P., W.F., A.S., H.M., S.C. and B.W. conceived the methodology. F.P.B., I.Y.B., T.P., W.F., A.S. and D.G. performed the investigation. F.P.B., I.Y.B., M.R., T.P., J.W., S.C. and B.W. wrote and edited the manuscript and figures.

References

1. Bershteyn, M., Nowakowski, T.J., Pollen, A.A., Di Lullo, E., Nene, A., Wynshaw-Boris, A. and Kriegstein, A.R. (2017) Human iPSC-derived cerebral organoids model cellular features of lissencephaly and reveal prolonged mitosis of outer radial glia. *Cell Stem Cell.*, **20**, 435–449. doi:10.1016/j.stem.2016.12.007
2. Branchu, J., Boutry, M., Sourd, L., Depp, M., Leone, C., Corriger, A., Vallucci, M., Esteves, T., Matusiak, R., Dumont, M. *et al.* (2017) Loss of spatacsin function alters lysosomal lipid clearance leading to upper and lower motor neuron degeneration. *Neurobiol. Dis.*, **102**, 21–37. doi:10.1016/j.nbd.2017.02.007.
3. Brennand, K., Savas, J.N., Kim, Y., Tran, N., Simone, A., Hashimoto-Torii, K., Beaumont, K.G., Kim, H.J., Topol, A., Ladran, I. *et al.* (2015) Phenotypic differences in hiPSC NPCs derived from patients with schizophrenia. *Mol. Psychiatry*, **20**, 361–368. doi:10.1038/mp.2014.22.
4. Calegari, F., Haubensak, W., Haffner, C. and Huttner, W.B. (2005) Selective lengthening of the cell cycle in the neurogenic subpopulation of neural progenitor cells during mouse brain development. *J. Neurosci.*, **25**, 6533–6538. doi:10.1523/JNEUROSCI.0778-05.2005.
5. Camp, J.G., Badsha, F., Florio, M., Kanton, S., Gerber, T., Wilsch-Bräuninger, M., Lewitus, E., Sykes, A., Hevers, W., Lancaster, M. *et al.* (2015) Human cerebral organoids recapitulate gene expression programs of fetal neocortex development. *Proc. Natl. Acad. Sci. U. S. A.*, **112**, 15672–15677. doi:10.1073/pnas.1520760112.

6. Chailangkarn, T., Trujillo, C.A., Freitas, B.C., Hrvoj-Mihic, B., Herai, R.H., Yu, D.X., Brown, T.T., Marchetto, M.C., Bardy, C., McHenry, L. *et al.* (2016) A human neurodevelopmental model for Williams syndrome. *Nature*, **536**, 338–343. doi:10.1016/j.neuroimage.2010.06.010.
7. Chang, J., Lee, S. and Blackstone, C. (2014) Spastic paraplegia proteins spastizin and spatacsin mediate autophagic lysosome reformation. *J. Clin. Invest.*, **124**, 5249–5262. doi:10.1172/JCI77598DS1.
8. Chuang, D.-M., Wang, Z. and Chiu, C.-T. (2011) GSK-3 as a target for lithium-induced neuroprotection against excitotoxicity in neuronal cultures and animal models of ischemic stroke. *Front. Mol. Neurosci.*, **4**, 15. doi:10.3389/fnmol.2011.00015.
9. Compagnucci, C., Petrini, S., Higuraschi, N., Trivisano, M., Specchio, N., Hirose, S., Bertini, E. and Terracciano, A. (2015) Characterizing PCDH19 in human induced pluripotent stem cells (iPSCs) and iPSC-derived developing neurons: emerging role of a protein involved in controlling polarity during neurogenesis. *Oncotarget*, **6**, 26804–26813. doi:10.18632/oncotarget.5757.
10. Denora, P.S., Smets, K., Zolfanelli, F., Ceuterick-de Groote, C., Casali, C., Deconinck, T., Sieben, A., Gonzales, M., Züchner, S., Darios, F. *et al.* (2016) Motor neuron degeneration in spastic paraplegia 11 mimics amyotrophic lateral sclerosis lesions. *Brain*, **139**, 1723–1734. doi:10.1093/brain/aww061.
11. Duan, X., Chang, J.H., Ge, S., Faulkner, R.L., Kim, J.Y., Kitabatake, Y., Liu, X.-B., Yang, C.-H., Jordan, J.D., Ma, D.K. *et al.* (2007) Disrupted-in-schizophrenia 1 regulates integration of newly generated neurons in the adult brain. *Cell*, **130**, 1146–1158. doi:10.1016/j.cell.2007.07.010.
12. Faigle, R. and Song, S. (2013) Signaling mechanisms regulating adult neural stem cells and neurogenesis. *Biochim. Biophys. Acta.*, **1830**, 2435–2448. doi:10.1016/j.bbagen.2012.09.002.
13. Götz, M. and Huttner, W.B. (2005) The cell biology of neurogenesis. *Nat. Rev. Mol. Cell Biol.*, **6**, 777–788. doi:10.1038/nrm1739.
14. Havlicek, S., Kohl, Z., Mishra, H.K., Prots, I., Eberhardt, E., Denguir, N., Wend, H., Plötz, S., Boyer, L., Marchetto, M.C.N. *et al.* (2014) Gene dosage-dependent rescue of HSP neurite defects in SPG4 patients' neurons. *Hum. Mol. Genet.*, **23**, 2527–2541, doi:10.1093/hmg/ddt644.
15. Hehr, U., Bauer, P., Winner, B., Schüle, R., Olmez, A., Koehler, W., Uyanik, G., Engel, A., Lenz, D., Seibel, A. *et al.* (2007) Long-term course and mutational spectrum of spatacsin-linked spastic paraplegia. *Ann. Neurol.*, **62**, 656–665. doi:10.1002/ana.21310.
16. Hur, E.M. and Zhou, F.Q. (2010) GSK3 signalling in neural development. *Nat. Rev. Neurosci.*, **11**, 539–551.
17. Ilouz, R., Kowalsman, N., Eisenstein, M. and Eldar-Finkelman, H. (2006) Identification of novel glycogen synthase kinase-3beta substrate-interacting residues suggests a common mechanism for substrate recognition. *J. Biol. Chem.*, **28**, 30621–30630.
18. Lancaster, M.A., Renner, M., Martin, C.-A., Wenzel, D., Bicknell, L.S., Hurles, M.E., Homfray, T., Penninger, J.M., Jackson, A.P. and Knoblich, J.A. (2013) Cerebral organoids model human brain development and microcephaly. *Nature*, **501**, 373–379. doi:10.1038/nature12517.
19. Lovestone, S., Boada, M., Dubois, B., Hüll, M., Rinne, J.O., Huppertz, H.-J., Calero, M., Andrés, M.V., Gómez-Carrillo, B., León, T., del Ser, T. and ARGO investigators (2015) A phase II trial of tideglusib in Alzheimer's disease. *J. Alzheimers Dis.*, **45**, 75–88. doi:10.3233/JAD-141959.
20. Mao, Y., Ge, X., Frank, C.L., Madison, J.M., Koehler, A.N., Doud, M.K., Tassa, C., Berry, E.M., Soda, T., Singh, K.K. *et al.* (2009) Disrupted in schizophrenia 1 regulates neuronal progenitor proliferation via modulation of GSK3beta/beta-catenin signaling. *Cell*, **136**, 1017–1031. doi:10.1016/j.cell.2008.12.044.
21. Mansour, A.A., Gonçalves, J.T., Bloyd, C.W., Li, H., Fernandes, S., Quang, D., Johnston, S., Parylak S.L., Jin, X., Gage, F.H. (2018) An in vivo model of functional and vascularized human brain organoids. *Nat. Biotechnol.*, **36**, 432–441. doi:10.1038/nbt.4127.
22. Marchetto, M.C., Belinson, H., Tian, Y., Freitas, B.C., Fu, C., Vadodaria, K., Beltrao-Braga, P., Trujillo, C.A., Mendes, A.P.D., Padmanabhan, K. *et al.* (2017) Altered proliferation and networks in neural cells derived from idiopathic autistic individuals. *Mol. Psychiatry*, **22**, 820–835. doi:10.1038/mp.2016.95.
23. Marchetto, M.C.N., Carromeu, C., Acab, A., Yu, D., Yeo, G.W., Mu, Y., Chen, G., Gage, F.H. and Muotri, A.R. (2010) A model for neural development and treatment of Rett syndrome using human induced pluripotent stem cells. *Cell*, **143**, 527–539. doi:10.1016/j.cell.2010.10.016.
24. Mariani, J., Coppola, G., Zhang, P., Abyzov, A., Provini, L., Tomasini, L., Amenduni, M., Szekely, A., Palejev, D., Wilson, M. *et al.* (2015) FOXG1-dependent dysregulation of GABA/glutamate neuron differentiation in autism spectrum disorders. *Cell*, **162**, 375–390. doi:10.1016/j.cell.2015.06.034.
25. Mishra, H.K., Prots, I., Havlicek, S., Kohl, Z., Pérez-Brangulí, F., Boerstler, T., Anneser, L., Minakaki, G., Wend, H., Hampl, M. *et al.* (2016) GSK3ß-dependent dysregulation of neurodevelopment in SPG11-patient induced pluripotent stem cell model. *Ann. Neurol.*, **79**, 826–840. doi:10.1111/j.1471-4159.2007.05194.x.
26. Montecchiani, C., Pedace, L., Lo Giudice, T., Casella, A., Mearini, M., Gaudiello, F., Pedroso, J.L., Terracciano, C., Caltagirone, C., Massa, R. *et al.* (2015) ALS5/SPG11/KIAA1840 mutations cause autosomal recessive axonal Charcot–Marie–Tooth disease. *Brain*, **139**, 73–85. doi:10.1093/brain/awv320.
27. Noctor, S.C., Martínez-Cerdeño, V., Ivic, L. and Kriegstein, A.R. (2004) Cortical neurons arise in symmetric and asymmetric division zones and migrate through specific phases. *Nat. Neurosci.*, **7**, 136–144. doi:10.1038/nn1172.
28. Orlacchio, A., Babalini, C., Borreca, A., Patrono, C., Massa, R., Basaran, S., Munhoz, R.P., Rogaeva, E.A., St George-Hyslop, P.H., Bernardi, G. and Kawarai, T. (2010) SPATACSIN mutations cause autosomal recessive juvenile amyotrophic lateral sclerosis. *Brain*, **133**, 591–598. doi:10.1093/brain/awp325.
29. Ortega, F., Berninger, B. and Costa, M.R. (2013) Primary culture and live imaging of adult neural stem cells and their progeny. *Methods Mol. Biol.*, **1052**, 1–11. doi:10.1007/7651_2013_22.
30. Parr, C., Carzaniga, R., Gentleman, S.M., Van Leuven, F., Walter, J. and Sastre, M. (2012) Glycogen synthase kinase 3 inhibition promotes lysosomal biogenesis and autophagic degradation of the amyloid-β precursor protein. *Mol. Cell. Biol.*, **32**, 4410–4418. doi:10.1128/MCB.00930-12.
31. Pensato, V., Castellotti, B., Gellera, C., Pareyson, D., Ciano, C., Nanetti, L., Salsano, Piscosquito, G., Sarto, E., Eoli, M. *et al.* (2014) Overlapping phenotypes in complex spastic paraplegias SPG11, SPG15, SPG35 and SPG48. *Brain*, **137**, 1907–1920.
32. Pérez-Brangulí, F., Mishra, H.K., Prots, I., Havlicek, S., Kohl, Z., Saul, D., Rummel, C., Dorca-Arevalo, J., Regensburger, M., Graef, D. *et al.* (2014) Dysfunction of spatacsin leads to axonal

pathology in SPG11-linked hereditary spastic paraplegia. *Hum. Mol. Genet.*, **23**, 4859–4874. doi:10.1093/hmg/ddu200.

33. Pilaz, L.-J. and Silver, D.L. (2015) Post-transcriptional regulation in corticogenesis: how RNA-binding proteins help build the brain. *Wiley Interdiscip. Rev. RNA*, **6**, 501–515. doi:10.1002/wrna.1289.
34. Qian, X., Nguyen, H.N., Song, M.M., Hadiono, C., Ogden, S.C., Hammack, C., Yao, B., Hamersky, G.R., Jacob, F., Zhong, C. *et al.* (2016) Brain-region-specific organoids using mini-bioreactors for modeling ZIKV exposure. *Cell*, **165**, 1238–1254. doi:10.1016/j.cell.2016.04.032.
35. Renvoisé, B., Chang, J., Singh, R., Yonekawa, S., FitzGibbon, E.J., Mankodi, A., Vanderver, A., Schindler, A., Toro, C., Gahl, W.A. *et al.* (2014) Lysosomal abnormalities in hereditary spastic paraplegia types SPG15 and SPG11. *Ann. Clin. Transl. Neurol.*, **1**, 379–389. doi:10.1002/acn3.64.
36. Stevanin, G., Santorelli, F.M., Azzedine, H., Coutinho, P., Chomilier, J., Denora, P.S., Martin, E., Ouvrard-Hernandez, A.-M., Tessa, A., Bouslam, N. *et al.* (2007) Mutations in SPG11, encoding spatacsin, are a major cause of spastic paraplegia with thin corpus callosum. *Nat. Genet.*, **39**, 366–372. doi:10.1038/ng1980.
37. Stromillo, M.L., Malandrini, A., Dotti, M.T., Battaglini, M., Borgogni, F., Tessa, A., Storti, E., Denora, P.S., Santorelli, F.M., Gaudiano, C. *et al.* (2011) Structural and metabolic damage in brains of patients with SPG11-related spastic paraplegia as detected by quantitative MRI. *J. Neurol.*, **258**, 2240–2247. doi:10.1007/s00415-011-6106-x.
38. Takahashi, K., Tanabe, K., Ohnuki, M., Narita, M., Ichisaka, T., Tomoda, K. and Yamanaka, S. (2007) Induction of pluripotent stem cells from adult human fibroblasts by defined factors. *Cell*, **131**, 861–872. doi:10.1016/j.cell.2007.11.019
39. Varga, R.-E., Khundadze, M., Damme, M., Nietzsche, S., Hoffmann, B., Stauber, T., Koch, N., Hennings, J.C., Franzka, P., Huebner, A.K. *et al.* (2015) In vivo evidence for lysosome depletion and impaired autophagic clearance in hereditary spastic paraplegia type SPG11. *PLoS Genet.*, **11**, e1005454. doi:10.1371/journal.pgen.1005454.